https://doi.org/10.5194/egusphere-2026-3665
Preprint. Discussion started: 12 August 2026

An aircraft-based Bayesian inversion of Berlin CO_2 emissions with explicit background treatment

Lukas Pilz[1], Christopher Lüken-Winkels[1], Alina Fiehn[2], Anke Roiger[2], and Sanam N. Vardag[1,3]

[1]Institute of Environmental Physics, Heidelberg University, Heidelberg, Germany
[2]Deutsches Zentrum für Luft- und Raumfahrt, Institut für Physik der Atmosphäre, Oberpfaffenhoffen, Germany
[3]Heidelberg Centre for the Environment, Heidelberg University, Heidelberg, Germany

Correspondence: Lukas Pilz (lukas.pilz@iup.uni-heidelberg.de) and Sanam N. Vardag (sanam.vardag@uni-heidelberg.de)

Abstract. Quantifying greenhouse gas (GHG) emissions from urban areas is critical for assessing progress toward climate goals. Aircraft-based measurements provide valuable information on urban emission fluxes; however, their interpretation is often limited by uncertainties in atmospheric background concentrations. Here, we present an emission estimate of Berlin city emissions that explicitly includes background concentrations from a Eulerian background run as state vector elements in a Bayesian inversion framework. Using data from the 20[th] of July flight of the 2018 3DO aircraft campaign of the [UC][2] ("Urban Climates Under Change") project over Berlin and high-resolution GHG and meteorological simulations using Weather Research and Forecasting (WRF) model, we derive a CO_2 emission estimate for the city of Berlin. We find an optimized Berlin emission rate of $13.4 \pm 4.6\,\mathrm{MtCO_2 a^{-1}}$. The emissions rate is about $48\,\%$ higher than the prior total annual emissions of the TNO anthropogenic bottom-up inventory (time-scaled emissions, $10.8\,\mathrm{MtCO_2 a^{-1}}$) and VPRM biogenic (time-varying, -$1.7\,\mathrm{MtCO_2 a^{-1}}$) and about $30\,\%$ of the estimate from the traditional mass balance approach ($44 \pm 24\,\mathrm{MtCO_2 a^{-1}}$), while reducing the uncertainty by over a factor of five. We verify our posterior background concentration with independent concentration measurements above the boundary layer. This study provides an improved independent estimate of urban emissions and demonstrates that explicit treatment of background concentrations in inversions improves aircraft-based urban flux estimates.

1 Introduction

Urban areas account for the majority of anthropogenic CO_2 emissions and are therefore key targets for mitigation and monitoring efforts. Accurately quantifying urban CO_2 emissions at high spatial and temporal resolution is essential to track mitigation progress and inform policy. Independent assessments of urban emissions require inference from atmospheric measurements rather than sole reliance on bottom-up emission inventories. However, a measurement-based approach to urban emissions remains challenging due to a combination of the large and variable uncertainties in atmospheric transport, and the diffuse and temporally variable emissions over a comparatively large area. Additionally, the difficult separation of local enhancements from a background signal, and the limited sampling in time and space further complicate the emission estimation.

Several complementary observational strategies have emerged to address this challenge, which can be broadly grouped into space-based remote sensing and ground-based measurements. Space-based retrievals of column-averaged CO_2 (XCO2) from dedicated missions such as GOSAT, OCO-2 and S5P have demonstrated the capability to resolve plumes from individual power plants and megacities (Nassar et al., 2017; Reuter et al., 2019), and the upcoming Copernicus Anthropogenic CO_2 Monitoring (CO2M) constellation has been designed specifically for systematic monitoring of anthropogenic emissions at the city and facility scale (Kuhlmann et al., 2019). While satellite observations are inherently scalable across many cities, the small column enhancement over urban areas relative to the atmospheric background, sensitivity to clouds and aerosols, and revisit times of several days to weeks currently limit their utility for continuous monitoring and for resolving short-term emission variability (Kuhlmann et al., 2019; Reuter et al., 2019). Ground-based remote sensing approaches such as in Paris (Vogel et al., 2019) and in Munich (Dietrich et al., 2021) are cheaper to deploy, however they suffer from similar problems regarding signal magnitude and can only retrieve total column values. Complementing these measurements are ground-based in-situ approaches such as eddy-covariance measurements (Christen et al., 2011; Turnbull et al., 2015; Lauvaux et al., 2016; Molinier et al., 2026) or networks in various cities like Los Angeles (Verhulst et al., 2017), Salt Lake City (Kunik et al., 2019), Paris (Staufer et al., 2016; Lian et al., 2024; Ponomarev et al., 2026), Zurich (Grange et al., 2025), Berkeley (Shusterman et al., 2016; Turner et al., 2016), or Munich (Aigner et al., 2026), which provide continuous, high-precision measurements at sub-hourly resolution. In Lüken-Winkels et al. (2026), the authors show that ground-based in-situ networks will aid independent urban emissions monitoring and will likely be able to help reduce the large uncertainties of emission inventories. However, the spatial representativeness of the networks is constrained by the limited number of stations and their proximity to heterogeneous near-surface sources within the urban canopy, which can strongly bias inferred city-wide fluxes and if not carefully treated can pose issues, as they are not able to directly and homogeneously sample the urban plume downwind of the city (Li et al., 2026). Airborne in-situ measurements represent a middle ground between these approaches: a single flight can sample an urban plume across horizontal scales of tens of kilometers and vertically probe the full depth of the boundary layer, integrating signals from broad upwind source regions while avoiding the strong local heterogeneity that affects surface observations (Cambaliza et al., 2014; Pitt et al., 2019; Klausner et al., 2020; Lopez-Coto et al., 2020; Kostinek et al., 2021; Luther et al., 2022; Hajny et al., 2023). At the same time, aircraft campaigns are resource-intensive and provide only snapshots in time, so extracting the maximum information from each flight is essential.

Traditional methods for estimating city emissions from aircraft measurements often rely on mass-balance approaches that subtract a chosen background and attribute the residual enhancement to sources inside the domain (Cambaliza et al., 2014; Pitt et al., 2019; Hajny et al., 2023). Those approaches are simple and intuitive, but they depend strongly on how the background is defined and typically assume spatial homogeneity or steady transport over the sampling period (Klausner et al., 2020). The resulting sensitivity to background choice and transport errors can produce substantial and difficult-to-quantify uncertainty in inferred emissions; Klausner et al. (2020) report that plausible alternative background constructions shift the inferred CO_2 flux of Berlin by nearly 50 %. Urban inversion frameworks can help address these limitations by combining observations, transport models, and prior emissions while explicitly considering error covariances. Nevertheless, the treatment of background concentrations remains a source of uncertainty.

High-resolution aircraft-based inversions have been successfully used for CH_4 and CO_2 fluxes at regional and urban scales (Lauvaux et al., 2016; Lopez-Coto et al., 2020; Pitt et al., 2019; Staufer et al., 2016), and urban applications have explored multiple strategies for constructing or optimizing background inflow fields. In particular, Lopez-Coto et al. (2020) jointly optimize a

https://doi.org/10.5194/egusphere-2026-3665
Preprint. Discussion started: 12 August 2026

time-varying background together with fluxes for the Washington–Baltimore area, demonstrating that explicitly representing the inflow field can alter inferred emissions and uncertainty estimates, especially when observations are sparse or winds are weak.

In this study, we optimize the CO_2 emissions of Berlin based on aircraft measurements from 2018 by explicitly including the background concentration field as part of the state vector within a Bayesian inversion. We analyze the 3DO aircraft campaign as part of the $[UC]^2$ ("Urban Climates Under Change") project around Berlin in July 2018: airborne in-situ CO_2 and CH_4 measurements were collected by German Aerospace Center (DLR) using a Cessna 208B equipped with a Picarro cavity ring-down spectrometer (CRDS) on 5 days between the 16th and 26th of July 2018. We compare results from (i) the conventional mass-balance approach conducted by Klausner et al. (2020), and (ii) the Bayesian inversion with and without an augmented state vector that includes background fields and to (iii) bottom-up inventories. We use the most comprehensively sampled flight (20th of July 2018) as a proof-of-concept case to examine the benefits and limitations of the respective approaches. Our study explicitly provides an independent validation of the optimized posterior background against in-situ observations above the planetary boundary layer from the same flight that were not assimilated into the inversion. We additionally introduce a prior-correlation inflation scheme designed to prevent the local plume signal from being absorbed into the posterior background, quantify the flux-uncertainty incurred through our prior uncertainty estimate using a dedicated sensitivity experiment, and compare the results to an inversion where the background is held fixed rather than jointly optimized. We close with a discussion of implications for future aircraft campaigns and urban monitoring strategies.

2 Data and Methods

2.1 Aircraft Campaign

The aircraft observations analyzed in this study were collected during the Urban Climate Under Change ($[UC]^2$) campaign around Berlin in July 2018 (Scherer et al., 2019; Klausner et al., 2020). The campaign used the DLR Cessna 208B Grand Caravan, equipped with the METPOD meteorological sensor suite and a Picarro G1301-m CRDS measuring CO_2, CH_4, and H_2O. The instrument characteristics and measurement uncertainties are presented in Klausner et al. (2020). Five research flights were conducted between 16th and 26th of July 2018, each comprising upwind and downwind transects of the Berlin metropolitan area to capture urban plume enhancements. The flight on 20th of July 2018 provided a coherent sampling of the Berlin urban plume, with a clearly defined boundary layer and well-mixed boundary-layer air. Flights on the other days are not considered, as the urban plume was either not captured or the boundary layer was not clearly separated (18th, 23rd, 24th, 25th July). The aforementioned flight is therefore used as the representative case for emission optimization. Its flight path is shown in Figure 1. The aircraft performed one upwind transect northwest of Berlin, a corkscrew vertical profile over the Tempelhofer Feld inside the city, and three downwind transects southeast of the urban area.

https://doi.org/10.5194/egusphere-2026-3665
Preprint. Discussion started: 12 August 2026

2.2 Meteorological and Model Data

As a source of meteorological and prior concentration fields, we use the MACRO-2018 dataset (Pilz et al., 2025).

The MACRO-2018 dataset contains hourly simulated meteorology as well as CO_2 and CO concentrations for the whole year of 2018. It comprises five focus-domains in German Metropolitan Areas (Berlin, Rhine-Main-Neckar, Rhine-Ruhr, Nuremberg and Munich) simulated at $1\,\mathrm{km}$ resolution which are nested in a Germany domain at $5\,\mathrm{km}$ and a Europe domain at $15\,\mathrm{km}$ resolution. The vertical resolution is 42 layers with 14 levels below $1.5\,\mathrm{km}$, similarly to previous studies like Lian et al. (2018). The dataset contains two whole WRF simulations, one using the MYJ and another using the YSU boundary-layer schemes. A comparison of these two simulations gives us a first-order estimate of model transport uncertainty.

This dataset combines $1\,\mathrm{km}$-resolution meteorological WRF simulations with CO_2 and CO dispersion simulations. It uses the WRF-Chem model in tracer mode to calculate concentration fields from underlying biogenic CO_2 fluxes from the Vegetation Photosynthesis and Respiration Model (VPRM) (Glauch et al., 2025) and anthropogenic CO_2 and CO fluxes from the TNO GHGco v4.1 inventory. Apart from the 3-D meteorological fields, the dataset includes forward-modeled CO_2 and CO concentration enhancements within the domain, and a respective background value as initial and boundary condition (from CAMS experiment ID gqpe — IFS cycle CY43R1). The concentration data the background field is using is generated from CAMS simulations assimilating data from the Greenhouse Gases Observing Satellite (GOSAT) measured by the Thermal and Near infrared Sensor for Carbon Observation (TANSO) instrument.

Within the inversion, these meteorological fields are used to calculate footprints using the Lagrangian Particle Dispersion Model FLEXPART-WRF (Brioude et al., 2013). This model uses gridded meteorology to integrate the dispersion of pseudo-tracers spawned at a particular measurement point in space and time. These tracers are then integrated backwards in time. The resulting "footprint" is a 4D scalar field, which serves as measure for the sensitivity of the measurement to the respective grid cells. Our footprints are sampled by 10000 pseudo-particles per measurement which are integrated backwards in time for 24 hours, resembling the settings in (Lüken-Winkels et al., 2026). The measurements for which these footprints are calculated are spaced at intervals of 5 minutes along the flight track. Because we also perform a background estimation in parallel to the emissions estimation, we need prior background concentration information for all measurements. These prior background concentrations are provided by MACRO-2018, which includes a first estimate thereof using the previously mentioned background concentration field from outside the Europe domain.

2.3 Bottom-up inventories

Several bottom-up emission inventories are available for Berlin and the surrounding region for the year 2018 or nearby years. The self-reported Berlin emissions are $15.7\,\mathrm{MtCO_2a^{-1}}$ and are provided annually by Amt für Statistik Berlin-Brandenburg (2025) and represent the officially reported fossil fuel CO_2 emissions within the administrative city boundaries. These data are available only as annual totals without spatial, temporal, or sectoral disaggregation. Klausner et al. (2020) additionally compared the aircraft measurements to the CAMS-REG v5.1 inventory (Kuenen et al., 2014) and the EDGAR v6.0 database (Crippa et al., 2020), both of which provide anthropogenic CO_2 emissions for 2015 at $0.1° \times 0.1°$ and $0.0625° \times 0.125°$ resolution, but

https://doi.org/10.5194/egusphere-2026-3665
Preprint. Discussion started: 12 August 2026

lack temporally explicit information beyond annual means. They give an annual emission estimate of 22.6 and 24.2 $\mathrm{MtCO_2a^{-1}}$ for the Berlin city district, respectively.

For the MACRO-2018 simulations and our inversion approach, we use the TNO GHGco v4.1 inventory (Super et al., 2020), which provides gridded emissions for 2018 at 1 km resolution and includes sector-specific temporal scaling factors that allow for month-in-year, day-in-week, and hour-in-day emission variability. This feature makes it particularly suitable as a dynamic prior for our inversion framework. While the annual average equals 15.3 $\mathrm{MtCO_2a^{-1}}$ for TNO, the time-factor corrected value for the flight day is 10.8 $\mathrm{MtCO_2a^{-1}}$. Differences in the emission inventories arise from variations in input data, emission factors, spatial proxies, and temporal downscaling methods. As shown by Ahn et al. (2023), relative uncertainties in city-scale CO_2 inventories can exceed 50 %, highlighting the difficulty of accurately capturing local emission processes and sectoral activity data and emphasizing the importance of measurement-based constraints.

In addition to anthropogenic fluxes, we include biogenic CO_2 fluxes from the Vegetation Photosynthesis and Respiration Model (VPRM) (Mahadevan et al., 2005; Glauch et al., 2025). During the July 2018 campaign period, the VPRM fluxes indicate daytime CO_2 uptake of approximately 1.7 $\mathrm{MtCO_2a^{-1}}$ across the Berlin domain, implying that biogenic fluxes play a minor role in the overall urban carbon balance during this period. The bottom-up estimate (prior) of total emissions (anthropogenic and biogenic) equals $9.1 \pm 6.8\,\mathrm{MtCO_2a^{-1}}$.

2.4 Traditional Mass Balance Method

The mass balance approach is a well-established method for estimating urban emissions from aircraft measurements. It derives CO_2 fluxes by integrating the product of horizontal wind speed and observed plume enhancements across a vertical cross-section downwind of the city. The method assumes steady meteorological conditions with horizontally homogeneous inflow, a well-mixed boundary layer, and negligible storage changes within the domain.

$$f = \int_0^{\mathrm{PBLH}} \mathrm{d}z \int_a^b \mathrm{d}x \left(c(x,z) - c_{\mathrm{bck}}(x,z)\right) \frac{p(x,z)}{T(x,z)\cdot R} M \cdot u(x,z) \tag{1}$$

The flux according to the mass balance method is calculated using Eq. 1 with R and M being the ideal gas constant and molar mass, $p(x,z)$ and $T(x,z)$ being the observed pressure and temperature, $c(x,z)$ and $c_{\mathrm{bck}}(x,z)$ the measured concentration and background concentration and $u(x,z)$ the wind component perpendicular to the flux plane. Background mole fractions are typically derived from upwind transects, either through linear interpolation or by using air-parcel back trajectories.

Klausner et al. (2020) apply a mass balance approach to the aircraft data from July 20th, yielding a total emission rate of $44 \pm 24\,\mathrm{MtCO_2a^{-1}}$. They attribute the large uncertainties of this estimate primarily to variability in wind-direction, uncertainty in PBL-height, and the determination of background concentrations. Further details are provided in Klausner et al. (2020). This estimate of urban CO_2 emissions is substantially higher than the TNO inventory for the flight period, particularly when accounting for the net biospheric impact (VPRM estimate: 1.7 $\mathrm{MtCO_2a^{-1}}$). However, given the large uncertainty associated

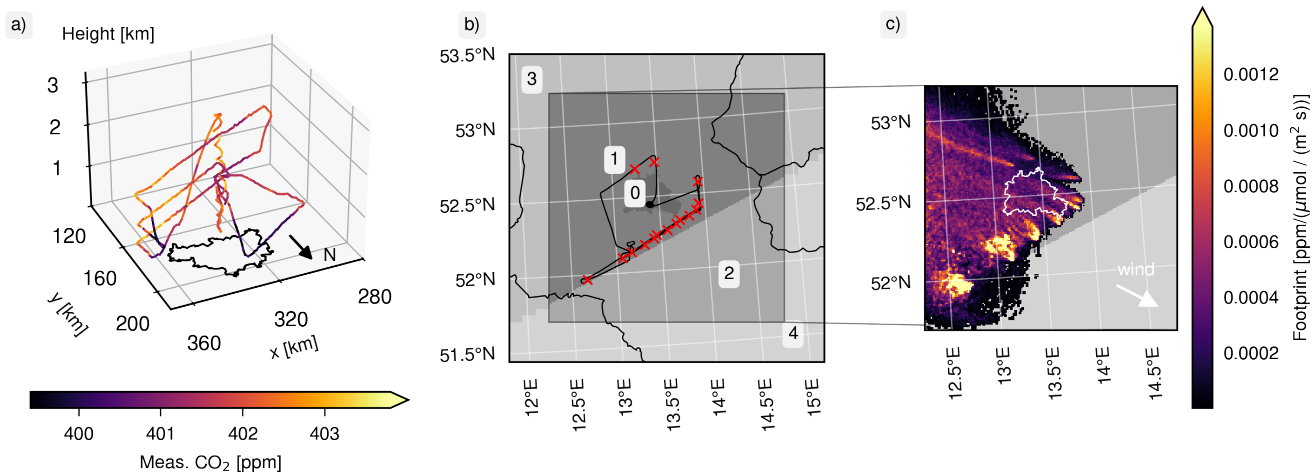

Figure 1. a) Aircraft flight track showing the upwind transect northwest of Berlin, the corkscrew vertical profile and the three downwind transects southeast of Berlin. b) Flight path used for the inversion and set-up of the state vector showing the five elements: Berlin city (0), Berlin upwind (1), Berlin downwind (2), Germany upwind (3) and Germany downwind (4). The footprint release points are shown as red crosses, c): Sensitivity of measurements as given by footprints from release points.

with the mass-balance approach, the estimate remains consistent with the EDGAR and CAMS-REG inventory estimates within error bounds.

2.5 Bayesian Inversion Framework

To overcome some of the limitations of the mass-balance approach, we perform a Bayesian inversion that jointly optimizes CO_2 emissions in 5 regions (i.e. Berlin city (0), Berlin upwind (1), Berlin downwind (2), Germany upwind (3) and Germany downwind (4)), as well as the background concentrations. The flight path and state vector set-up together with the aggregated footprint are shown in Figure 1. This state vector set-up allows us to determine the emissions of Berlin city under unknown background conditions. The inversion relates observed mole-fraction enhancements to emissions and background concentration through a linearized forward model

$$y = Kx + \epsilon \tag{2}$$

where y is is the vector of measured CO_2 mole fractions, x contains both emission scaling factors and background offsets, K is the forward model (Jacobian) and ϵ represents model-data mismatch error.

The first part of the forward model K refers to the emissions and contains a footprint f_{m_i,c_j} i.e. the contribution of emissions from grid cell c_j to observation m_i, which are aggregated from $1 \times 1\,\mathrm{km}$ cells balanced to the spatial resolution of the state vector (see Eq. 2). Footprints were initialized every $5\,\mathrm{min}$ along the flight track and integrated backwards in time for $24\,\mathrm{h}$. Along the transects, this temporal spacing corresponds to an approximate horizontal distance of $10\,\mathrm{km}$ between release points.

https://doi.org/10.5194/egusphere-2026-3665
Preprint. Discussion started: 12 August 2026

The second part of the forward model represents the background concentration at each measurement location. As a first estimate, we use the `CO2_BCK` field of MACRO-2018, which includes the boundary conditions at the European domain from CAMS concentrations. The inversion then adjusts these initial background values to account for additional contributions from fluxes between the edge of the footprints and the model domain boundary.

The resulting forward operator therefore has a block structure, where each measurement is expressed as the sum of an emission-driven enhancement and a background term:

$$\begin{pmatrix} m_0 \\ m_1 \\ \vdots \end{pmatrix} = \begin{pmatrix} f_{m0,c0} & f_{m0,c1} & \cdots & 1 & 0 & \cdots \\ f_{m1,c0} & f_{m1,c1} & & 0 & 1 & \\ & \vdots & \ddots & \vdots & & \ddots \end{pmatrix} \begin{pmatrix} e_{c0} \\ e_{c1} \\ \vdots \\ b_{m0} \\ b_{m1} \\ \vdots \end{pmatrix} + \epsilon \quad (3)$$

The state vector therefore contains 5 emission scaling factors (one per region) and N_m background offsets (one per assimilated measurement), for a total dimension of $5+N_m$. The Jacobian $\mathbf{K}$ is an $N_m \times (5+N_m)$ matrix whose left block contains the aggregated footprint sensitivities of each measurement to the five emission regions and whose right block is the $N_m \times N_m$ identity, associating each measurement with its own background element. The prior covariance $\mathbf{S}_a$ is block-diagonal, composed of a 5×5 emission block (Sect. 2.5.1) and an $N_m \times N_m$ background block.

Assuming Gaussian errors, the posterior state vector $\hat{x}$ and its posterior covariance $\hat{S}$ are obtained analytically following Rodgers (2000):

$$\hat{x} = x_a + \mathbf{S}_a\mathbf{K}^T\left(\mathbf{K}\mathbf{S}_a\mathbf{K}^T + \mathbf{S}_e\right)^{-1}(y - \mathbf{K}x_a) \quad (4)$$

$$\hat{\mathbf{S}} = (\mathbf{K}^T{\mathbf{S}_e}^{-1}\mathbf{K} + {\mathbf{S}_a}^{-1})^{-1} \quad (5)$$

where x_a and $\mathbf{S}_a$ denote the prior state vector and its covariance and $\mathbf{S}_e$ the model-data mismatch covariance, which are described in Sec. 2.5.1.

In order to gain a better understanding of the problem one can define the Gain and Average Kernel matrices. While the Gain matrix shows the influence of the additional measurement information on the posterior state vector, the Averaging Kernel matrix indicates the distance of the posterior state vector between prior and true state following Rodgers (2000):

$$\hat{x} = x_0 + \mathbf{G}(y - \mathbf{K}x_0) \quad (6)$$

$$= (\mathbb{1} - \mathbf{A})x_0 + \mathbf{G}y \quad (7)$$

$$= \mathbf{A}x_{true} + (\mathbb{1} - \mathbf{A})x_0 + \mathbf{G}\epsilon \quad (8)$$

While an ideal Averaging Kernel matrix would be an identity matrix, Averaging Kernel matrices with entries exceeding the $[-1,1]$ range are considered non-physical.

https://doi.org/10.5194/egusphere-2026-3665
Preprint. Discussion started: 12 August 2026

Prior fluxes are a combination of anthropogenic fluxes which are taken from the TNO GHGco v4.1 inventory and biogenic fluxes from the VPRM model.

2.5.1 Covariance Structure

There are two covariance matrices for our problem, which we will discuss separately, the model-data mismatch and the prior covariance matrix. We will start with the model-data mismatch covariance.

This covariance is constructed from a combination of the model and the measurement uncertainty. As a first-order estimate, we use the two separate simulations with two different boundary layer schemes which are included in the MACRO-2018 dataset. This average inter-physics difference between MYJ and YSU configurations of MACRO-2018 yields a model-induced concentration uncertainty of 0.49 ppm for the aircraft measurements used. The instrumental precision of the Picarro G1301-m of 0.15 ppm is used as the measurement uncertainty (Klausner et al., 2020). Combining these contributions using sum of squares yields a model-data mismatch uncertainty of 0.51 ppm.

The prior covariance matrix can be split into an emissions and a background concentration part. To find the uncertainty of the prior emissions in Berlin city, we conduct a sensitivity analysis. We run our inversion with Berlin city uncertainties of 25, 50, 75, 100, and 125 $\%$ (see Fig. A1) and find that above 75 $\%$, the results become physically unsound as the off-diagonals exceed $[-1, 1]$. Therefore, we choose 75 $\%$ as the uncertainty of the prior emissions in Berlin city.

The uncertainties of the other state vector elements are scaled relative to the Berlin cell based on the size of the state vector elements using sum of squares of gridcell-based inventory uncertainties which are provided by TNO. Note that since these grid-cell-based uncertainties do not account for temporal or height associated uncertainties, they therefore cannot be used as a complete prior uncertainty estimate and are thus used only in a relative sense.

Background concentration uncertainties are estimated from the temporal variability of the MACRO-2018 background field (75 min around the measurement). These uncertainties are inflated by 0.5 ppm to allow for adjustments of the background, accounting for fluxes between the edge of the footprints and the boundaries of the European domain which would otherwise not be captured. We determine the correlation of the background state vector elements by analyzing the correlation of the background concentration time series and use this value as a lower bound. We further increase the correlation among the individual background concentrations so that the correlation of the background to the measurements does not increase between prior and posterior (0.46 on average). This is performed to avoid imprinting the local enhancements measured during the flight onto the posterior background concentration estimate, which is expected to vary on larger temporal scales.

3 Results

3.1 Evaluation of model transport

We evaluate the meteorology and CO_2 enhancements of the MACRO-2018 dataset against the $[UC]^2$ aircraft observations to assess whether both the meteorological fields and the transport of prior emissions are suitable for use in the optimization. Model

https://doi.org/10.5194/egusphere-2026-3665
Preprint. Discussion started: 12 August 2026

Table 1. Mean absolute bias comparison of MACRO-2018 variables to flight measurements for the July 20th 2018 vertical profile. Separated into values below and above 2 km altitude.

	below 2 km		above 2 km	
	MYJ	YSU	MYJ	YSU
θ [K]	0.2	0.1	1.3	1.2
RH [%]	3.4	3.4	23.0	20.8
wind speed [m/s]	1.3	1.4	1.1	1.1
CO_2 v2 [ppm]	0.6	0.7	1.9	2.1

output was sampled in space and time along the aircraft flight path on 20 July 2018, and the extracted data were compared directly to the in-situ measurements.

Panel a) in Figure 2 shows the comparison of measured CO_2 mole fractions with the simulated concentrations from MACRO-2018 (using the VPRM biogenic emissions) for the two planetary boundary layer (PBL) schemes, MYJ and YSU. Both simulations fit the measurement well with the largest deviation occurring during the vertical profile (hatched part). The mean biases and bias-corrected mean absolute biases between the two simulations are similar to one another. Between the PBL schemes, the MYJ configuration yields a slightly lower mean bias (by about 0.2 ppm) than YSU. The largest deviations occur during the vertical spiral profile over Tempelhofer Feld, where observed concentrations reflect strong vertical gradients not fully resolved in the model.

The observed vertical profile exhibits a pronounced capping inversion at $2737 \pm 2\,\mathrm{m}$ (Klausner et al., 2020), typical of summertime convective conditions over Berlin. The model reproduces the general structure well up to about 2 km but underestimates and smooths the mixing-layer height, likely due to limited vertical resolution (cf. Table 1). Above this altitude deviations increase, reflecting the low vertical resolution of the model and uncertainty in boundary layer structure (cf. Table 1). Consequently, the simulated CO_2 concentrations do not capture the distinct peak associated with plume entrainment into the capping inversion at the top of the PBL seen in the observations. Above the PBL, simulated concentrations are overestimated, indicating that the large-scale background in MACRO-2018 is slightly too high. Both PBL schemes reproduce the thermodynamic structure of the boundary layer well, but differences arise in wind speed and mixing depth. The MYJ scheme shows slightly better agreement with observed wind speeds (mean bias $1.3\,\mathrm{ms^{-1}}$ below 2 km) than YSU ($1.4\,\mathrm{ms^{-1}}$) and therefore provides a more consistent basis for the inversion. It is thus used to drive the footprint calculations and prior background sampling.

Since the highest measurements included in the inversion are at 1.6 km and the observed meteorology and CO_2 concentrations match well with observations up to 2 km, this comparison indicates that the MACRO-2018 dataset is sufficiently accurate for the inversion. Remaining discrepancies, particularly in the upper PBL and free-tropospheric background, highlight the importance of jointly optimizing the background field.

https://doi.org/10.5194/egusphere-2026-3665
Preprint. Discussion started: 12 August 2026

3.2 Optimized CO_2 emissions and background CO_2

We calculate footprints of the observations along the upwind and downwind transects, consistent with the measurements used in the mass balance estimate of Klausner et al. (2020). These observations are expected to contain the most information for the inversion. We further exclude measurements that exhibit negative prior correlations in background concentrations, as the background of a single air mass is, by definition, positively correlated. This filtering ensures that the assumption of a smooth background field from a single air-mass is satisfied for all included measurements. After filtering, $N_m = 15$ measurements are included in the inversion. As input concentration values, we use a $20\,\mathrm{s}$ rolling average of the measured CO_2 concentration values, corresponding to an effective averaging length of approximately $1\,\mathrm{km}$, consistent with the model resolution.

We use an inversion setup similar to Lüken-Winkels et al. (2026). In order to perform the analytical Bayesian Inversion, we use the python package `pyinverse` (Maiwald et al., 2025). Input and output processing are performed using the python script `FlexWrfInversion` (commit `30ce5b89` between v0.1.3 and v0.1.4; https://github.com/ATMO-IUP-UHEI/FlexWrfInversion/). Run scripts for FLEXPART-WRF and postprocessing its output can be found in the FlexWrf python package (v0.1.4; https://github.com/ATMO-IUP-UHEI/FlexWrf/releases/tag/v0.1.5). And as stated previously, the meteorological data to drive FLEXPART-WRF is from MACRO-2018 (Pilz et al., 2025).

Applying the inversion, we find a posterior CO_2 emission for the Berlin city cell of $13.4 \pm 4.3\,\mathrm{MtCO_2a^{-1}}$. We quantify the uncertainty introduced through the sensitivity study by using the maximum difference in emissions estimation between 50, 75, and 100 % ($1.5\,\mathrm{MtCO_2a^{-1}}$). This yields a final emissions estimate for Berlin of $13.4 \pm 4.3\,\mathrm{MtCO_2a^{-1}}$, up from a prior emissions estimate of $9.1 \pm 6.8\,\mathrm{MtCO_2a^{-1}}$. The relative emission changes amount to +47.7 % for the Berlin city cell and +31.5 % for the Berlin upwind cell, while all other cells show much smaller adjustments. The posterior CO_2 emissions field shows the largest error reduction in Berlin city cell and its upwind neighbor (36.6 to 57.7 %), corresponding to the regions of highest sensitivity in the measurement footprints (cmp. Fig. 1).

The inversion adjusts the background concentrations downwards from approximately $403.5 \pm 0.5\,\mathrm{ppm}$ to $402.4 \pm 0.3\,\mathrm{ppm}$, while reducing its uncertainty by about half. This is achieved without increasing its correlation to the observations (prior and posterior correlation both 0.46). The downward adjustment is physically consistent, as the background concentrations between the outer footprint boundaries and the larger European domain are expected to be slightly lower, reflecting predominantly negative fluxes in these regions. The resulting posterior background concentration of $402.4 \pm 0.3\,\mathrm{ppm}$ closely agrees with the median of the observed CO_2 mixing ratios above the planetary boundary layer (402.6 ppm; cf. Fig. 3). These free-tropospheric values represent the far-field background of the sampled air masses, which are largely unaffected by local emissions. It is noteworthy that this background correction emerges solely from measurements within the boundary layer (up to $1.6\,\mathrm{km}$), as the measurements from the corkscrew flight pattern are not assimilated. Yet the inferred posterior background aligns remarkably well with independent observations above the mixing layer height (see Fig. 2). This agreement provides a strong indication of the robustness of the inversion framework.

The averaging kernel matrix (Fig. 3d) quantifies the sensitivity of the posterior state to the true state, providing a measure of how strongly the inversion is constrained by the observations rather than by the prior. Values close to unity along the diagonal

https://doi.org/10.5194/egusphere-2026-3665
Preprint. Discussion started: 12 August 2026

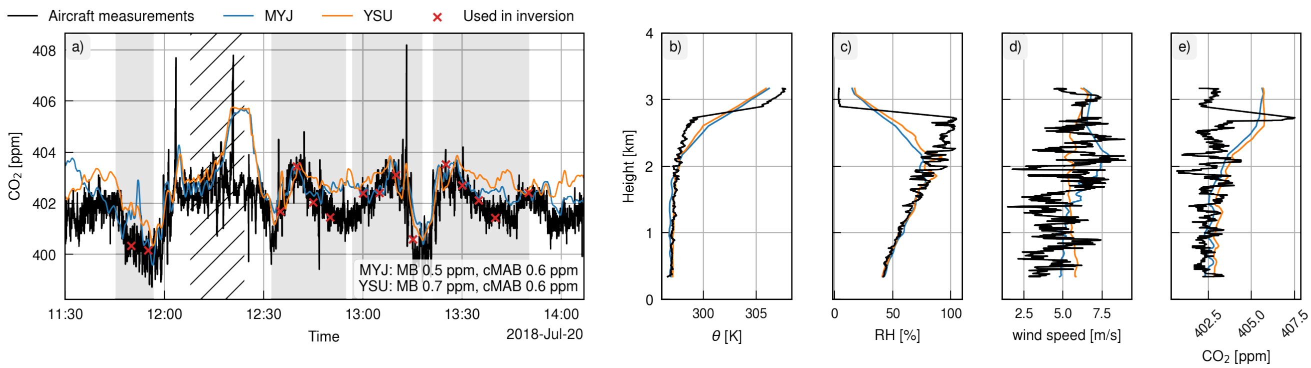

Figure 2. a) Comparison of measured and modeled CO_2 concentrations along the whole flight track. Shaded areas are upwind and downwind transects, hatched area is vertical profile. We find generally good agreement between measurement and model along the transects with Mean Biases (MB) of 0.5 and 0.7 ppm and bias-corrected MAB of 0.5 ppm for both simulations. Panels b) to e) show a comparison of modeled and measured variables along the vertical profile. The variables shown are (from left to right) potential temperature, relative humidity, wind speed, and CO_2 concentration. There is very good agreement between model and observations up to 2 km, with larger deviations above, likely due to the coarse vertical resolution of the simulation.

indicate that the corresponding grid cells are well resolved by the available data, whereas low or off-diagonal values reflect limited or spatially mixed information.

The averaging kernel matrix reveals that the diagonal elements corresponding to the Berlin city and Berlin upwind cell (0 and 1) are close to unity, indicating that the inversion system is well constrained in these areas. However, the off-diagonal terms between the Berlin city (C0), the Berlin upwind (C1), and the Germany upwind (C3) cells are comparatively large, implying that these regions are not fully independent of each other. This cross-sensitivity results from overlapping footprints and a limited number of measurements, which restricts the ability to fully disentangle the emission signals from the individual cells. The averaging kernel diagonals corresponding to the other regions is low as expected due to the poor sensitivities.

The gain matrix (Fig. 3e), in turn, represents the sensitivity of the posterior state to the measurements and thus illustrates which observations contribute most to constraining the solution. The highest gain values are found for the downwind transects (DW1–DW3), consistent with their large footprint sensitivities over the Berlin city cell. Furthermore, looking at Fig. 4, we find that the inversion adjusts the posterior concentrations so that the deviation from the measurements decreases.

3.3 Influence of Background Optimization on the Inversion

A key aspect of our inversion framework is the explicit inclusion of background concentration values as part of the state vector (see Sect. 2.4). To assess the importance of this design choice, we conducted a sensitivity experiment in which the prior background uncertainty was set to zero, effectively fixing the background to its prior value from the MACRO-2018 dataset (Pilz

https://doi.org/10.5194/egusphere-2026-3665
Preprint. Discussion started: 12 August 2026

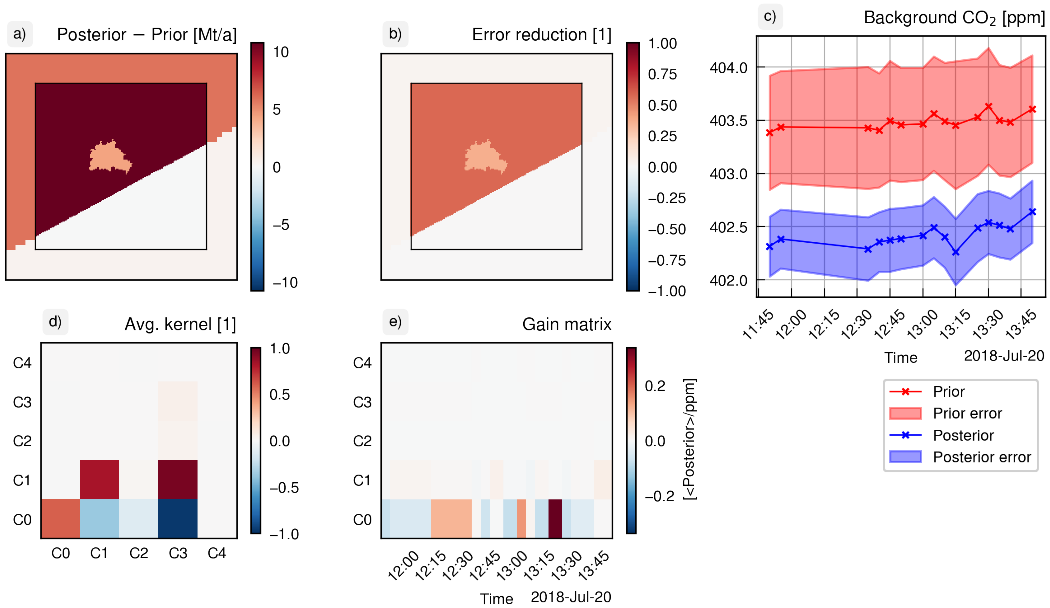

Figure 3. a) Difference of posterior emissions to prior emissions in Mt/a (47.7 % for Berlin, 31.5 % for Berlin upwind). b) Error reduction of 36.6 % for Berlin and 57.7 % for Berlin upwind. c) Prior and posterior background concentrations, showing a substantial downward shift in the posterior due to the inversion. d) Averaging kernel of inversion: diagonal elements are close to one while there are large off-diagonal elements for the upwind Germany cell. e) Gain matrix shows large impact of measurements on Berlin city cell.

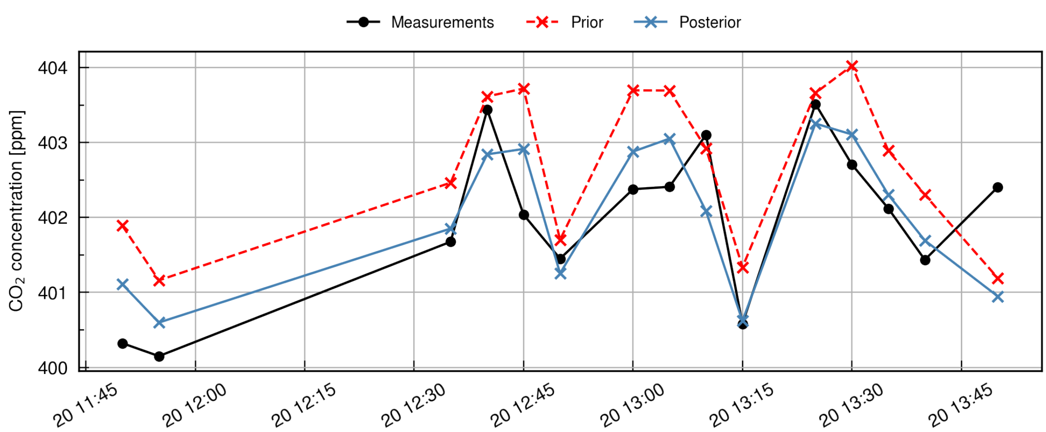

Figure 4. Comparison of prior and measured concentrations with concentrations optimized by the inversion. Deviations from measurements decrease due to assimilation of measurements in inversion.

https://doi.org/10.5194/egusphere-2026-3665
Preprint. Discussion started: 12 August 2026

et al., 2025). In this configuration, the inversion could only adjust the emissions field, while the background contributed as a fixed offset to the simulated concentrations.

The outcome of this test highlights the critical role of jointly assimilating the background and emissions. Figure 5 shows the resulting residuals and the degraded fit to the aircraft observations when the background is excluded from the optimization. When the background concentration is held fixed, the inversion yields a posterior emission estimate of $7.9 \pm 4.0\,\mathrm{MtCO_2a^{-1}}$, which is approximately $40\,\%$ lower than the estimate obtained when the background is optimized simultaneously, although both estimates still agree within their uncertainties. This systematic underestimation arises because part of the urban enhancement signal is attributed to an overestimated background. Furthermore, elements of the averaging kernel exceed $[-1, 1]$, indicating a loss of physical consistency in the inversion. The experiment demonstrates that optimizing the background field is essential for correctly partitioning observed concentration variations between background and local emissions. Accordingly, including the background as part of the state vector substantially improves both the accuracy and robustness of the inversion results.

4 Discussion

Aircraft-based studies are particularly sensitive to assumptions about the atmospheric background, which often constitute the largest single source of uncertainty in city-scale emission estimates (Lauvaux et al., 2016; Lopez-Coto et al., 2020; Klausner et al., 2020). Existing inversion frameworks have addressed this challenge in different ways: Lauvaux et al. (2016) use wind-direction-dependent tower measurement as prescribed background for Indianapolis, Lopez-Coto et al. (2020) optimize a time-varying background jointly with fluxes for Washington–Baltimore but do not independently validate the resulting posterior background. In traditional approaches, such as the mass-balance method applied by Klausner et al. (2020), background concentrations are subtracted a priori using upwind transects or regional model output. This relies on the assumption that the background field is spatially homogeneous and temporally stationary. These conditions are rarely met in complex summertime boundary layers, which can lead to substantial uncertainties in flux estimates. Our results show that explicitly representing the background field within a Bayesian inversion framework, together with independent constraints from free-tropospheric observations, substantially reduces these uncertainties.

By including background concentrations as part of the state vector, the inversion system can partition observed concentration variability into local emission signals and large-scale background gradients. The sensitivity test in Sect. 3.3 highlights the importance of this design choice: constraining the background field (i.e. removing its degrees of freedom) results in a $40\,\%$ underestimation of the posterior emissions. This demonstrates that jointly optimizing the background and emissions is essential to avoid systematic errors inherent to simplified background subtraction methods.

Our posterior estimate for Berlin emissions of $13.4 \pm 4.3\,\mathrm{MtCO_2a^{-1}}$ is about $47\,\%$ larger than the prior estimate (cf. Fig. 6). It is, however, substantially lower than the values inferred from the mass-balance approach of Klausner et al. (2020), which yielded emissions approximately three times higher from the same data. This level of discrepancy is consistent with the findings of Pitt et al. (2019), who showed that mass-balance estimates can be strongly biased for cities whose emissions are not cleanly isolated from surrounding source regions — a condition that also applies to Berlin due to non-negligible upwind contributions

https://doi.org/10.5194/egusphere-2026-3665
Preprint. Discussion started: 12 August 2026

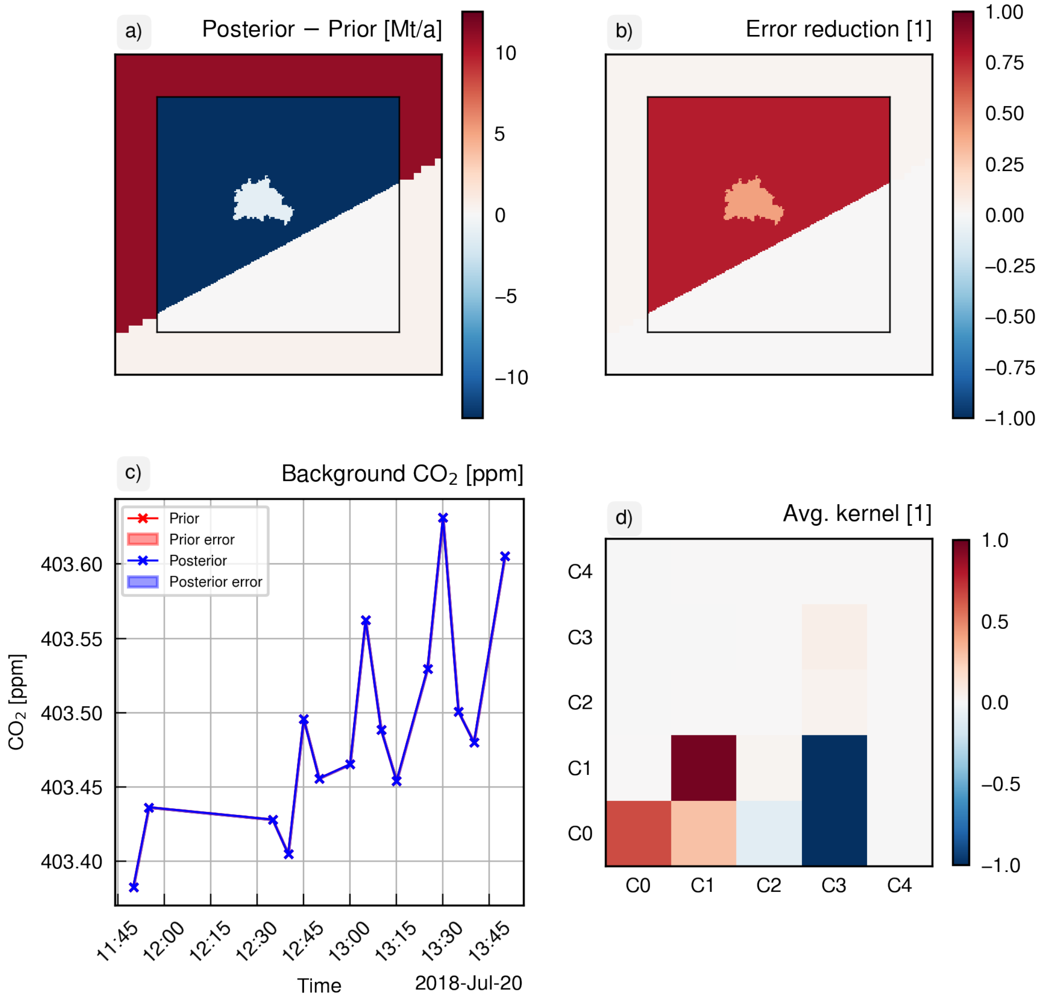

Figure 5. Results of inversion with background concentration uncertainty set to zero (only emissions optimization). Posterior is shifted downwards of prior, to $7.9 \pm 4.0\,\mathrm{MtCO_2a^{-1}}$. The off-diagonal elements of the Averaging Kernel far exceed $[-1,1]$.

https://doi.org/10.5194/egusphere-2026-3665
Preprint. Discussion started: 12 August 2026

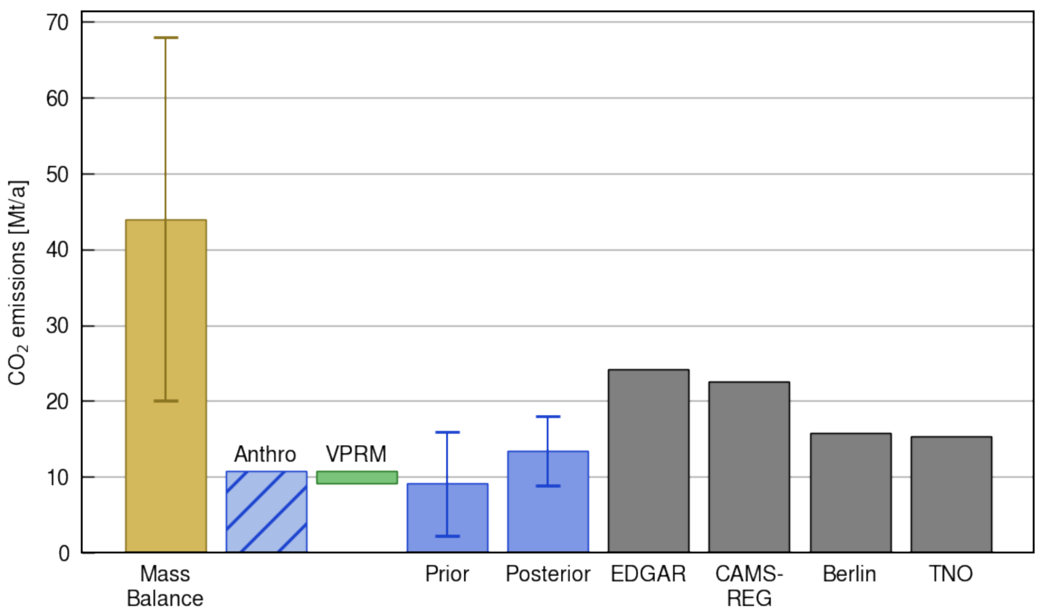

Figure 6. Comparison of emissions estimates for Berlin. Yellow bar is the mass balance estimate performed by T. Klausner, blue and green bars are from this study. Hatched blue bar is the anthropogenic prior emissions (TNO with timefactors) and green bar is biogenic prior (uptake from VPRM). Solid blue bars are prior and posterior emissions. Error reduction of 36.6 % clearly visible, error of posterior is factor five below mass balance error. Grey bars are average daily emissions from multiple sources including CAMS-REG, EDGAR, the City of Berlin and TNO.

from the broader German domain. A further contribution to this difference is the large footprint of the mass balance estimate which also includes sources outside of the city boundaries. Nevertheless, the inversion-induced increase relative to the prior is consistent between methods, suggesting either underestimated anthropogenic emissions or unaccounted biogenic respiration in the priors (or a combination of both). The posterior uncertainty of $\pm 4.6\,\mathrm{MtCO_2 a^{-1}}$ represents an error reduction by over a factor of five compared to the mass-balance estimate ($\pm 24\,\mathrm{MtCO_2 a^{-1}}$). The large uncertainty reported by Klausner et al. (2020) reflects their transparent and conservative treatment of the substantial background uncertainties inherent to applying a mass-balance approach under these non-ideal source-attribution conditions. This substantial uncertainty reduction highlights the ability of the Bayesian Inversion framework with explicit background estimation to more efficiently extract the available information from the aircraft observations.

Given the short-term nature of the aircraft observations, the resulting estimate is not representative of the full annual mean, which complicates comparisons with annual inventories such as EDGAR, CAMS-REG and the Berlin inventory. These inventories report emissions of 24.4, 22.6, and 15.7 $\mathrm{MtCO_2 a^{-1}}$ while the TNO annual average emission is 15.3 $\mathrm{MtCO_2 a^{-1}}$. Applying temporal scaling factors (hour-in-day, day-in-week, month-in-year) to the TNO emissions reduced their magnitude. However, these factors are averaged over the whole year and are not necessarily representative on the daily level. Using the

https://doi.org/10.5194/egusphere-2026-3665
Preprint. Discussion started: 12 August 2026

prior biogenic flux estimate as a baseline, our estimate suggests $15.1 \pm 4.3\,\mathrm{MtCO_2 a^{-1}}$ anthropogenic emissions on this particular day. While this is broadly consistent with the annual averages especially when considering increased winter emissions by heating, lower daily anthropogenic emissions are expected in summer. This implies that the TNO inventory underestimates annual mean emissions, or that a short-term event increased the emissions on the measurement day. Alternatively, higher total emissions could also reflect enhanced biogenic respiration or reduced photosynthetic uptake not properly captured in the VPRM model, and which cannot be effectively distinguished from anthropogenic emissions using total CO_2 only.

Future applications may extend this framework to multi-flight or multi-species inversions, potentially combining CO_2 with co-emitted tracers (e.g. CO, CH_4) or with isotopic constraints. The explicit treatment of background and uncertainty covariance makes this system flexible and scalable to aircraft campaigns in other urban regions.

5 Conclusions

We have developed and applied a Bayesian inversion framework that jointly optimizes urban CO_2 emissions and background concentrations using aircraft observations over Berlin from the 3DO data collected as part of the [UC]^2 campaign. This approach directly addresses one of the dominant error sources in aircraft-based flux estimation, namely the representation of the background. In particular, the inversion yields posterior CO_2 emissions for Berlin of $13.4 \pm 4.3\,\mathrm{MtCO_2 a^{-1}}$, which are higher than the prior but consistent with independent bottom-up inventories, and markedly lower than the mass-balance estimate by Klausner et al. (2020). We reduce the flux uncertainty by around a factor of five compared to the one in Klausner et al. (2020) ($\pm 24\,\mathrm{MtCO_2 a^{-1}}$), who identified the background uncertainty as the main error source. A sensitivity analysis of the prior uncertainty indicates an additional contribution of $\pm 1.5\,\mathrm{MtCO_2 a^{-1}}$ to the emissions uncertainty. Overall, the emissions uncertainty is reduced by more than a factor of five compared to the mass-balance approach.

The inclusion of background concentration in the state vector was shown to have a significant influence on the result, and independent observation above the PBL indicate that the posterior background concentration is effectively adjusted within the inversion. These findings demonstrate that the joint optimization of background concentrations and emissions substantially improves both the accuracy and interpretability of urban CO_2 inversions, and provides a framework for the evaluation of future aircraft campaigns.

Looking ahead, this framework can be extended to multi-day or multi-flight inversions once suitable campaign data are available, enabling temporal aggregation toward seasonal or annual emission estimates and increasing the statistical robustness beyond what a single flight can provide.

https://doi.org/10.5194/egusphere-2026-3665
Preprint. Discussion started: 12 August 2026

Appendix A

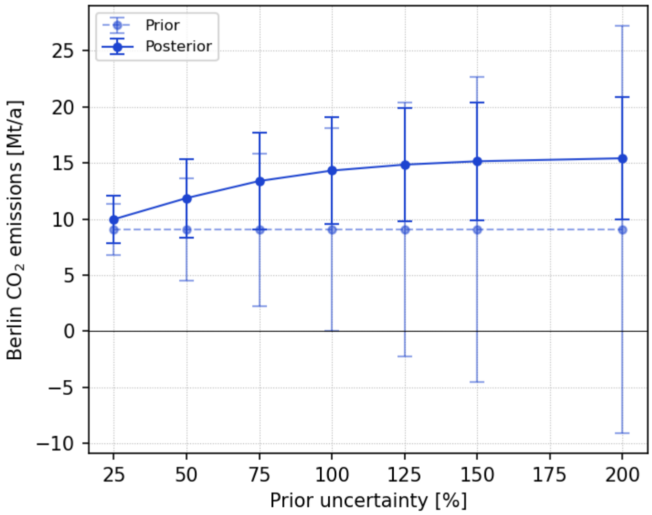

Figure A1. Sensitivity study showing prior and posterior emissions with associated base relative prior emissions uncertainties. Selected uncertainty was 75 %, as above this value the Averaging Kernel showed nonphysical behavior.

375

https://doi.org/10.5194/egusphere-2026-3665
Preprint. Discussion started: 12 August 2026

Code and data availability. Inversion result data available under https://doi.org/10.5281/zenodo.20964395. Code is available under https://doi.org/10.5281/zenodo.20964324.

Author contributions. **Lukas Pilz** — Conceptualization, Methodology, Software, Validation, Formal analysis, Investigation, Writing - Original Draft, Writing - Review & Editing, Visualization; **Christopher Lüken-Winkels** — Conceptualization, Methodology, Investigation, Writing - Review & Editing; **Alina Fiehn** — Measurement, Data Curation, Writing - Review & Editing; **Anke Roiger** — Writing - Review & Editing; **Sanam N. Vardag** — Conceptualization, Methodology, Investigation, Writing - Original Draft, Writing - Review & Editing, Resources, Supervision, Project Administration, Funding Acquisition

Competing interests. No competing interests are present.

Acknowledgements. This work is part of the joint project ITMS, funded by the German Federal Ministry of Research, Technology and Space (BMFTR) under reference number 01LK2102D. This project used computing resources of the German Climate Computation Center (DKRZ), granted by its Scientific Steering Committee (WLA) under project IDs bb1170 and bm1400. The German Federal Ministry of Education and Research (BMBF) funded the 3DO consortium and the DLR Cessna flights under grant 01LP1602 within the framework of Research for Sustainable Development (FONA; www.fona.de). The authors gratefully acknowledge the SDS@hd data storage service, supported by the Ministry of Science, Research and the Arts Baden-Württemberg (MWK). For the publication fee we acknowledge financial support by Heidelberg University. During the preparation of this work, large language models (LLMs) were used in a limited assistive manner for manuscript text and plotting scripts. No AI tools were used to generate, modify, or adjust the original scientific content presented.

https://doi.org/10.5194/egusphere-2026-3665
Preprint. Discussion started: 12 August 2026

References

Ahn, D., Goldberg, D., Coombes, T., Kleiman, G., and Anenberg, S.: CO2 emissions from C40 cities: citywide emission inventories and comparisons with global gridded emission datasets, Environmental Research Letters, 18, 034 032, https://doi.org/10.1088/1748-9326/acbb91, 2023.

Aigner, P., Chen, J., Böhm, F., Chariot, M., Emmenegger, L., Frölich, L., Grange, S., Kühbacher, D., Kürzinger, K., Laurent, O., et al.: ACROPOLIS: Munich urban CO2 sensor network, Atmospheric Measurement Techniques, 19, 745–773, https://doi.org/10.5194/amt-19-745-2026, 2026.

Amt für Statistik Berlin-Brandenburg: Energie- und CO_2-Bilanz, https://web.archive.org/web/20250927205413/https://download.statistik-berlin-brandenburg.de/7158c16f221e4d65/aa951a320938/energie-zeitreihe-2022-energiebilanz.xlsx, 2025.

Brioude, J., Arnold, D., Stohl, A., Cassiani, M., Morton, D., Seibert, P., Angevine, W., Evan, S., Dingwell, A., Fast, J. D., Easter, R. C., Pisso, I., Burkhart, J., and Wotawa, G.: The Lagrangian particle dispersion model FLEXPART-WRF version 3.1, Geoscientific Model Development, 6, 1889–1904, https://doi.org/10.5194/gmd-6-1889-2013, 2013.

Cambaliza, M. O. L., Shepson, P. B., Caulton, D. R., Stirm, B., Samarov, D., Gurney, K. R., Turnbull, J., Davis, K. J., Possolo, A., Karion, A., Sweeney, C., Moser, B., Hendricks, A., Lauvaux, T., Mays, K., Whetstone, J., Huang, J., Razlivanov, I., Miles, N. L., and Richardson, S. J.: Assessment of uncertainties of an aircraft-based mass balance approach for quantifying urban greenhouse gas emissions, Atmospheric Chemistry and Physics, 14, 9029–9050, https://doi.org/10.5194/acp-14-9029-2014, 2014.

Christen, A., Coops, N., Crawford, B., Kellett, R., Liss, K., Olchovski, I., Tooke, T., van der Laan, M., and Voogt, J.: Validation of modeled carbon-dioxide emissions from an urban neighborhood with direct eddy-covariance measurements, Atmospheric Environment, 45, 6057–6069, https://doi.org/10.1016/j.atmosenv.2011.07.040, 2011.

Crippa, M., Solazzo, E., Huang, G., Guizzardi, D., Koffi, E., Muntean, M., Schieberle, C., Friedrich, R., and Janssens-Maenhout, G.: High resolution temporal profiles in the Emissions Database for Global Atmospheric Research, Scientific data, 7, 121, https://doi.org/10.1038/s41597-020-0462-2, 2020.

Dietrich, F., Chen, J., Voggenreiter, B., Aigner, P., Nachtigall, N., and Reger, B.: MUCCnet: Munich Urban Carbon Column network, Atmospheric Measurement Techniques, 14, 1111–1126, https://doi.org/10.5194/amt-14-1111-2021, 2021.

Glauch, T., Marshall, J., Gerbig, C., Botía, S., Gałkowski, M., Vardag, S. N., and Butz, A.: pyVPRM: A next-generation Vegetation Photosynthesis and Respiration Model for the post-MODIS era, EGUsphere, https://doi.org/10.5194/egusphere-2024-3692, 2025.

Grange, S. K., Rubli, P., Fischer, A., Brunner, D., Hueglin, C., and Emmenegger, L.: The ZiCOS-M CO2 sensor network: measurement performance and CO2 variability across Zurich, Atmospheric Chemistry and Physics, 25, 2781–2806, https://doi.org/10.5194/acp-25-2781-2025, 2025.

Hajny, K. D., Lyon, D. R., Armstrong, A., Floerchinger, C. R., Jayarathne, T., Kaeser, R., Lavoie, T., Salmon, O. E., Stirm, B. H., Stuff, A. A., Tomlin, J. M., Wulle, B., Lopez-Coto, I., and Shepson, P. B.: Assessing the bias and uncertainties in the aircraft mass balance technique for the determination of carbon dioxide emission rates, Elementa: Science of the Anthropocene, 11, 00 135, https://doi.org/10.1525/elementa.2022.00135, 2023.

Klausner, T., Mertens, M., Huntrieser, H., Galkowski, M., Kuhlmann, G., Baumann, R., Fiehn, A., Jöckel, P., Pühl, M., and Roiger, A.: Urban greenhouse gas emissions from the Berlin area: A case study using airborne CO2 and CH4 in situ observations in summer 2018, Elem Sci Anth, 8, https://doi.org/10.1525/elementa.411, 2020.

Kostinek, J., Roiger, A., Eckl, M., Fiehn, A., Luther, A., Wildmann, N., Klausner, T., Fix, A., Knote, C., Stohl, A., and Butz, A.: Estimating Upper Silesian coal mine methane emissions from airborne in situ observations and dispersion modeling, Atmospheric Chemistry and Physics, 21, 8791–8807, https://doi.org/10.5194/acp-21-8791-2021, 2021.

Kuenen, J., Visschedijk, A., Jozwicka, M., and Denier Van Der Gon, H.: TNO-MACC_II emission inventory; a multi-year (2003–2009) consistent high-resolution European emission inventory for air quality modelling, Atmospheric Chemistry and Physics, 14, 10 963–10 976, https://doi.org/10.5194/acp-14-10963-2014, 2014.

Kuhlmann, G., Broquet, G., Marshall, J., Clément, V., Löscher, A., Meijer, Y., and Brunner, D.: Detectability of CO_2 emission plumes of cities and power plants with the Copernicus Anthropogenic CO_2 Monitoring (CO2M) mission, Atmospheric Measurement Techniques, 12, 6695–6719, https://doi.org/10.5194/amt-12-6695-2019, 2019.

Kunik, L., Mallia, D. V., Gurney, K. R., Mendoza, D. L., Oda, T., and Lin, J. C.: Bayesian inverse estimation of urban CO2 emissions: Results from a synthetic data simulation over Salt Lake City, UT, Elementa: Science of the Anthropocene, 7, https://doi.org/10.1525/elementa.375, 2019.

Lauvaux, T., Miles, N. L., Deng, A., Richardson, S. J., Cambaliza, M. O., Davis, K. J., Gaudet, B., Gurney, K. R., Huang, J., O'Keefe, D., Song, Y., Karion, A., Oda, T., Patarasuk, R., Razlivanov, I., Sarmiento, D., Shepson, P., Sweeney, C., Turnbull, J., and Wu, K.: High-resolution atmospheric inversion of urban CO2 emissions during the dormant season of the Indianapolis Flux Experiment (INFLUX), Journal of Geophysical Research: Atmospheres, 121, 5213–5236, https://doi.org/10.1002/2015jd024473, 2016.

Li, J., Li, P., Han, P., Cheng, Z., Li, J., Zhang, T., Chen, D., Zheng, Y., Zeng, N., and Zhang, G.: Advances in the design of urban CO2 emission monitoring networks: a review, Carbon Research, 5, 3, https://doi.org/10.1007/s44246-025-00239-z, 2026.

Lian, J., Wu, L., Bréon, F.-M., Broquet, G., Vautard, R., Zaccheo, T. S., Dobler, J., and Ciais, P.: Evaluation of the WRF-UCM mesoscale model and ECMWF global operational forecasts over the Paris region in the prospect of tracer atmospheric transport modeling, Elementa: Science of the Anthropocene, 6, https://doi.org/10.1525/elementa.319, 2018.

Lian, J., Laurent, O., Chariot, M., Lienhardt, L., Ramonet, M., Utard, H., Lauvaux, T., Bréon, F.-M., Broquet, G., Cucchi, K., Millair, L., and Ciais, P.: Development and deployment of a mid-cost CO2 sensor monitoring network to support atmospheric inverse modeling for quantifying urban CO2 emissions in Paris, Atmospheric Measurement Techniques, 17, 5821–5839, https://doi.org/10.5194/amt-17-5821-2024, 2024.

Lopez-Coto, I., Ren, X., Salmon, O. E., Karion, A., Shepson, P. B., Dickerson, R. R., Stein, A., Prasad, K., and Whetstone, J. R.: Wintertime CO2, CH4, and CO Emissions Estimation for the Washington, DC–Baltimore Metropolitan Area Using an Inverse Modeling Technique, Environmental Science & Technology, 54, 2606–2614, https://doi.org/10.1021/acs.est.9b06619, 2020.

Luther, A., Kostinek, J., Kleinschek, R., Defratyka, S., Stanisavljević, M., Forstmaier, A., Dandocsi, A., Scheidweiler, L., Dubravica, D., Wildmann, N., Hase, F., Frey, M. M., Chen, J., Dietrich, F., Nęcki, J., Swolkień, J., Knote, C., Vardag, S. N., Roiger, A., and Butz, A.: Observational constraints on methane emissions from Polish coal mines using a ground-based remote sensing network, Atmospheric Chemistry and Physics, 22, 5859–5876, https://doi.org/10.5194/acp-22-5859-2022, 2022.

Lüken-Winkels, C., Pilz, L., and Vardag, S. N.: Designing urban CO2 sensor networks under realistic uncertainties and biases: Results from synthetic studies in Berlin and Munich, Elementa: Science of the Anthropocene, 14, 00 118, https://doi.org/10.1525/elementa.2025.00118, 2026.

Mahadevan, P., Matross, D., Wofsy, S., Xiao, X., Lin, J., Gerbig, C., Chow, V., Gottlieb, E., and Munger, J.: Modeling Large-Scale Biosphere NEE by Integrating Satellite Images and Climate Data-Vegetation Photosynthesis and Respiration Model (VPRM), in: AGU Fall Meeting Abstracts, vol. 2005, pp. A41C–0055, 2005.

https://doi.org/10.5194/egusphere-2026-3665
Preprint. Discussion started: 12 August 2026

Maiwald, R., Lüken-Winkels, C., and Pilz, L.: ATMO-IUP-UHEI/pyinverse: v1.0.0, https://doi.org/10.5281/zenodo.17611367, 2025.

Molinier, B., Aigner, P., Brunner, D., Chen, J., Christen, A., Constantin, L., Denier van der Gon, H., Hilland, R., Kühbacher, D., Li, J., Maiwald, R., Super, I., Vardag, S. N., and Kljun, N.: Insights from the Convolution of Emission Inventories with Flux Footprints from Tall Eddy Covariance Towers at Three European Cities, ACS E&T Air, 3, 1664–1676, https://doi.org/10.1021/acsestair.6c00148, 2026.

Nassar, R., Hill, T. G., McLinden, C. A., Wunch, D., Jones, D. B. A., and Crisp, D.: Quantifying CO_2 Emissions From Individual Power Plants From Space, Geophysical Research Letters, 44, 10 045–10 053, https://doi.org/10.1002/2017GL074702, 2017.

Pilz, L., Denier van der Gon, H., Glauch, T., Marshall, J., and Vardag, S. N.: MACRO-2018 - High-Resolution Simulation of CO and CO2 concentrations over German Metropolitan Areas for 2018 using WRF-Chem, World Data Center for Climate (WDCC) at DKRZ, https://doi.org/10.26050/WDCC/MACRO-2018, 2025.

Pitt, J. R., Allen, G., Bauguitte, S. J.-B., Gallagher, M. W., Lee, J. D., Drysdale, W., Nelson, B., Manning, A. J., and Palmer, P. I.: Assessing London CO2, CH4 and CO emissions using aircraft measurements and dispersion modelling, Atmospheric Chemistry and Physics, 19, 8931–8945, https://doi.org/10.5194/acp-19-8931-2019, 2019.

Ponomarev, N., Steiner, M., Koene, E., Rubli, P., Grange, S., Constantin, L., Ramonet, M., David, L., Hamzehloo, A., Emmenegger, L., et al.: Estimation of CO2 fluxes in the cities of Zurich and Paris using the ICON-ART CTDAS inverse modelling framework, Atmospheric Chemistry and Physics, 26, 547–570, https://doi.org/10.5194/acp-26-547-2026, 2026.

Reuter, M., Buchwitz, M., Schneising, O., Krautwurst, S., O'Dell, C. W., Richter, A., Bovensmann, H., and Burrows, J. P.: Towards monitoring localized CO_2 emissions from space: co-located regional CO_2 and NO_2 enhancements observed by the OCO-2 and S5P satellites, Atmospheric Chemistry and Physics, 19, 9371–9383, https://doi.org/10.5194/acp-19-9371-2019, 2019.

Rodgers, C. D.: Inverse Methods for Atmospheric Sounding, WORLD SCIENTIFIC, https://doi.org/10.1142/3171, 2000.

Scherer, D., Ament, F., Emeis, S., Fehrenbach, U., Leitl, B., Scherber, K., Schneider, C., and Vogt, U.: Three-Dimensional Observation of Atmospheric Processes in Cities, Meteorologische Zeitschrift, pp. 121–138, https://doi.org/10.1127/metz/2019/0911, 2019.

Shusterman, A. A., Teige, V. E., Turner, A. J., Newman, C., Kim, J., and Cohen, R. C.: The BErkeley Atmospheric CO_2 Observation Network: initial evaluation, Atmospheric Chemistry and Physics, 16, 13 449–13 463, https://doi.org/10.5194/acp-16-13449-2016, 2016.

Staufer, J., Broquet, G., Bréon, F.-M., Puygrenier, V., Chevallier, F., Xueref-Rémy, I., Dieudonné, E., Lopez, M., Schmidt, M., Ramonet, M., Perrussel, O., Lac, C., Wu, L., and Ciais, P.: The first 1-year-long estimate of the Paris region fossil fuel CO2 emissions based on atmospheric inversion, Atmospheric Chemistry and Physics, 16, 14 703–14 726, https://doi.org/10.5194/acp-16-14703-2016, 2016.

Super, I., Dellaert, S. N. C., Visschedijk, A. J. H., and van der Gon, H. A. C. D.: Uncertainty analysis of a European high-resolution emission inventory of CO_2 and CO to support inverse modelling and network design, Atmospheric Chemistry and Physics, 20, 1795–1816, https://doi.org/10.5194/acp-20-1795-2020, 2020.

Turnbull, J. C., Sweeney, C., Karion, A., Newberger, T., Lehman, S. J., Tans, P. P., Davis, K. J., Lauvaux, T., Miles, N. L., Richardson, S. J., Cambaliza, M. O., Shepson, P. B., Gurney, K., Patarasuk, R., and Razlivanov, I.: Toward quantification and source sector identification of fossil fuel CO_2 emissions from an urban area: Results from the INFLUX experiment, Journal of Geophysical Research: Atmospheres, 120, 292–312, https://doi.org/10.1002/2014JD022555, 2015.

Turner, A. J., Shusterman, A. A., McDonald, B. C., Teige, V., Harley, R. A., and Cohen, R. C.: Network design for quantifying urban CO_2 emissions: assessing trade-offs between precision and network density, Atmospheric Chemistry and Physics, 16, 13 465–13 475, https://doi.org/10.5194/acp-16-13465-2016, 2016.

Verhulst, K. R., Karion, A., Kim, J., Salameh, P. K., Keeling, R. F., Newman, S., Miller, J., Sloop, C., Pongetti, T., Rao, P., Wong, C., Hopkins, F. M., Yadav, V., Weiss, R. F., Duren, R. M., and Miller, C. E.: Carbon dioxide and methane measurements from the Los Angeles

https://doi.org/10.5194/egusphere-2026-3665
Preprint. Discussion started: 12 August 2026

Megacity Carbon Project – Part 1: calibration, urban enhancements, and uncertainty estimates, Atmospheric Chemistry and Physics, 17, 8313–8341, https://doi.org/10.5194/acp-17-8313-2017, 2017.

Vogel, F. R., Frey, M., Staufer, J., Hase, F., Broquet, G., Xueref-Remy, I., Chevallier, F., Ciais, P., Sha, M. K., Chelin, P., Jeseck, P., Janssen, C., Té, Y., Groß, J., Blumenstock, T., Tu, Q., and Orphal, J.: XCO_2 in an emission hot-spot region: the COCCON Paris campaign 2015, Atmospheric Chemistry and Physics, 19, 3271–3285, https://doi.org/10.5194/acp-19-3271-2019, 2019.